CHAPTER II

LITERATURE REVIEW

2.1 Hydrogen storage in metal hydrides

Hydrogen chemisorption in the forms of metal and complex hydrides consists of dissociation of hydrogen molecule, diffusion of hydrogen atoms into interstitial sites of metal and formation of M-H bond (Figure 2.1(A)). Nucleation and growth of hydride will occur under moderate temperatures and pressures following the pressure-composition (PCT) isotherms (Figure 2.1(B)(i)) (Klebanoff, 2016). The PCT curve is the correlation between the equilibrium pressure and the hydrogen storage content at temperature settings. The α-phase region corresponds to the formation of metal hydride at low pressures. The plateau region is in accordance with the equilibrium of α and β phases. Nucleation and growth of the metal hydride refer to β-phase region. The plateau region in the PCT plot indicates the reversible hydrogen content. Considering van't Hoff equation (2.1), enthalpy (ΔH) and entropy (ΔS) of hydride formation can be obtained from slope and y-intercept of the van't Hoff plot (Figure 2.1(B)(ii).

$$\ln(P_{eq}/P_0) = \frac{\Delta H}{RT} - \frac{\Delta S}{RT} \quad (2.1)$$

Where P_{eq} is the plateau pressure, T is the temperature, P_0 is the reference pressure (1 bar), R is the gas constant (R = 8.314 J.mol^{-1}. K^{-1}), ΔH and ΔS are the enthalpy and entropy changes, respectively.

The enthalpy of metal hydrides relates to the heat during hydrogen absorption and desorption. To obtain equilibrium pressure (P_{eq}) of 1 bar at 40-150 °C, an operating

temperature of fuel cell, ΔH of 30– 55 kJ/mol with constant ΔS (130 J/mol K) is required (Züttle, 2008).

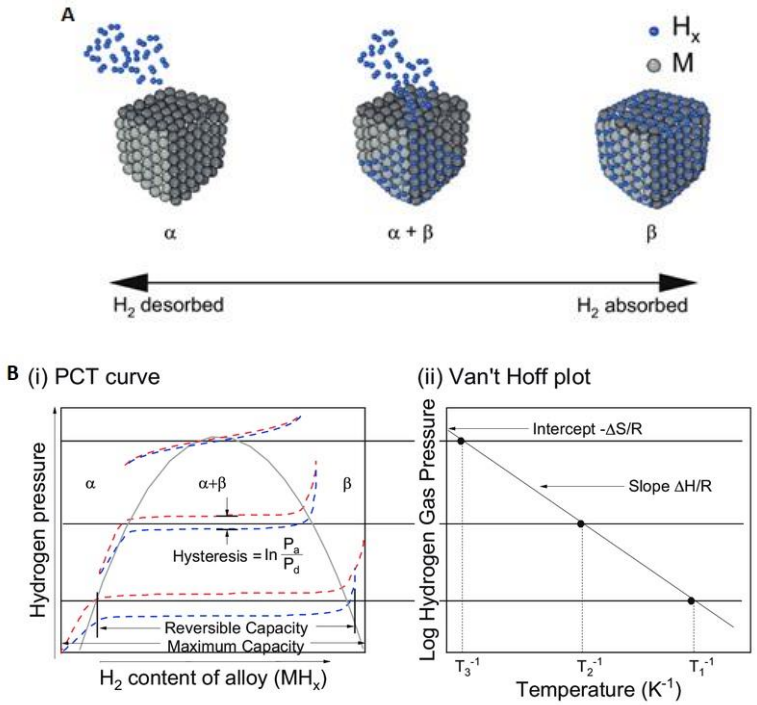

Figure 2.1 Hydride formation (**α** and **β** phase) (A), PCT curves (i) and van' t Hoff plot (ii) (B) (Modi et al., 2021).

Thus, metal hydrides with high hydrogen capacity and suitable thermodynamic properties are challenging for hydrogen storage materials. Another barrier for the practical application of metal hydrides is kinetic, considering a rate-limiting step for a particular reaction. From Figure 2.2(A), during absorption hydrogen gas is physisorption onto the surface of metal hydride (step 1). Then, hydrogen molecules dissociate into atoms, further occupying and penetrating into the interstitial sites of the host metal (steps 2 and 3). When the amount of hydrogen increases, diffusion through the hydride layer occurs (step 4) to complete hydride formation. For desorption, metal hydride decomposes into metal and hydrogen (step 1). Hydrogen atom diffuses through metal (step 2) and to the surface (step 3). Finally,

the recombination of hydrogen atoms into molecules (step 4), releasing to the environment (step 5).

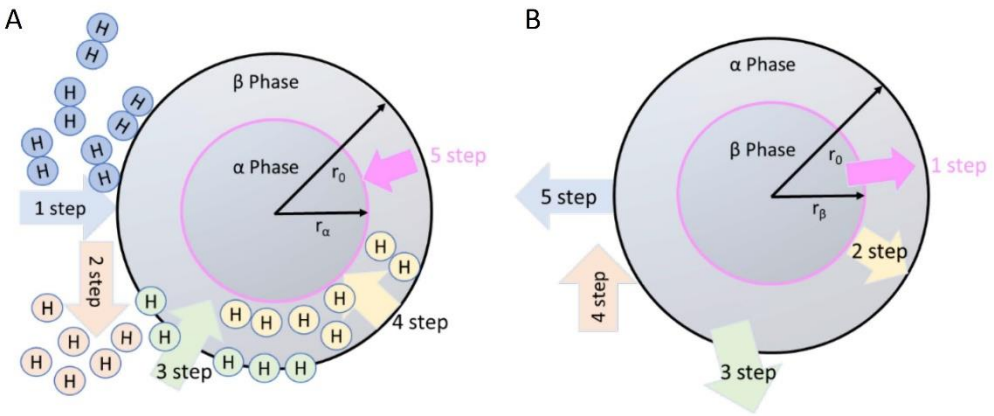

Figure 2.2 Steps for the absorption (A) and desorption (B) of the metal hydrides. (Jain et al., 2018).

The chemical reaction's activation energy (E_a) presents a barrier in the reaction pathway, in which many hydrides show significantly high Ea. To practically use metal hydride, rapid hydrogen de/rehydrogenation at moderate temperature is needed. Catalytic doping is of interest due to lowering Ea without any changes in chemical structures of reactants and products as well as thermodynamic properties (Züttle, 2008). Ea can be investigated by differential scanning calorimetry (DSC) technique and Kissinger equation (2.2).

$$\ln(\beta/T^2_p) = \frac{-Ea}{RTp} + \ln(k_0) \qquad (2.2)$$

where β is the heating rate (°C/min), Tp is the peak desorption temperature, R is the gas constant (8.314 J mol^{-1} K^{-1}), Ea is the activation energy, and k_0 is a constant.

2.2 $LiNH_2/Li_2NH$ and their tuning strategies

Although other metal hydrides and/or complex hydrides following Figure 1.5 have accomplished high gravimetric and volumetric hydrogen capacities, their dehydrogenation temperatures are still high due to the large enthalpy. $LiNH_2/Li_2NH$ system is one of the most competitive materials for hydrogen storage because of their suitable gravimetric and volumetric capacities according to the U.S. (DOE) (5.5 wt. % and 40 gH_2/L, respectively) (Partnership., 2017). $LiNH_2$ consists of Li^+ cation and NH_2^- anionic group with tetragonal by space group of *I-4*, which preferred an anti-fluorite with the arrangement of Li in a tetrahedral hole and N in a cubic close-packed. However, $LiNH_2$ decomposes into Li_2NH and NH_3 at 373-375 °C under vacuum (equation (2.3)) instead of hydrogen. Thus, $LiNH_2$-LiH composite has been proposed, which the obtained NH_3 further reacts with LiH to form Li_2NH and H_2 (equation (2.4)). However, the deterioration of LiH due to hydrolysis/oxidation led to NH_3 emission, resulting in poisoning proton exchange membranes (PEMFCs) and poor hydrogen capacity (Shaw et al., 2008). Moreover, poor kinetics due to slow NH_3 diffusion through the Li_2NH coated on the $LiNH_2$ core and deficient interfaces between LiH and NH_3 are serious issues (Chen et al., 2002). Regarding the previous work reported by Chen et al. (2003) and Chen et al. (2002), overall reaction for $LiNH_2$-LiH decomposition (equation (2.5)) provides the storage capacity of 6.5 wt. % H_2.

$$2LiNH_2 \rightarrow Li_2NH + NH_3 \quad (2.3)$$

$$2LiH + NH_3 \rightarrow Li_2NH + 2H_2 \quad (2.4)$$

$$LiNH_2 + LiH \rightarrow Li_2NH + H_2 \quad (2.5)$$

For Li_2NH, it has two crystal structures of *Fm-3m* and *Imma* space group as low-temperature (LT) and high-temperature (HT) phases, respectively (Juza, 1951). Phase transition of Li_2NH from the LT to the HT can be detected at 400-500 K. During the decomposition of $LiNH_2$, the rate-limiting step is NH_3 formation at the interface of $LiNH_2/Li_2NH$ (Figure 2.3).

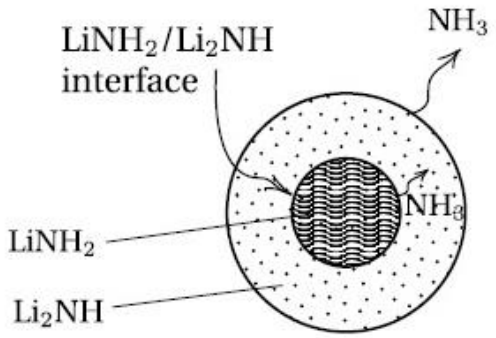

Figure 2.3 The decomposition path of the $LiNH_2/Li_2NH$ (Miceli et al., 2010).

Several approaches to improve de/rehydrogenation kinetics and suppress NH_3 emission of $LiNH_2$-LiH composites, including nanoparticle preparation and catalytic doping have been reported. Varin et al. (2010) studied the effects of milling time and $LiNH_2$: LiH molar ratio. When the milling time increased up to 25 h, the grain size of $LiNH_2$-LiH composite decreased, enhancing specific surface area. (Figure 2.4(A)).

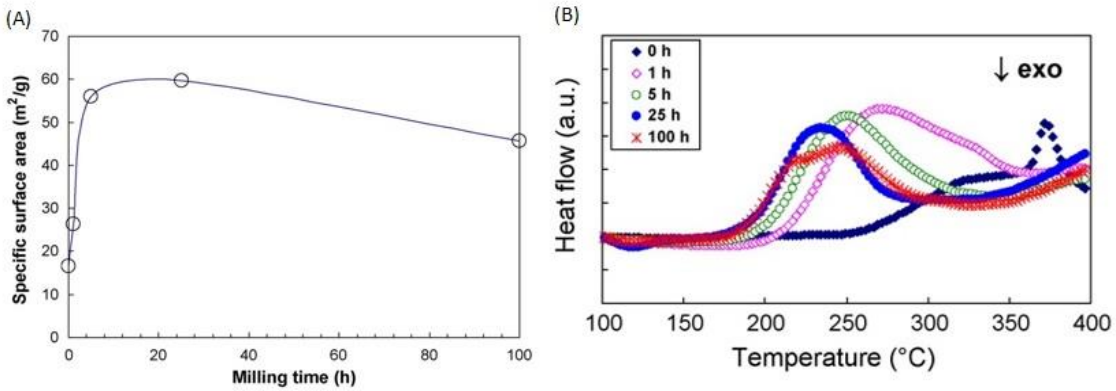

Figure 2.4 The specific surface area to ball milling time of the $LiNH_2$-LiH composite (A) and DSC profiles for varied milling time (B).

Dehydrogenation temperature decreased with the increase of milling time up to 25 h (Figure 2.4(B)). From Table 2.1, not only milling time but also the enhancement of LiH content benefits dehydrogenation kinetics.

Table 2.1 Summary of the DSC profiles for $LiNH_2$-LiH by varied milling time and LiH molar ratio.

	Molar ratio	DSC peak (°C)	
Milling time (h)	($LiNH_2$-LiH)	T (onset)	T (main)
0	1:1	268	324.7
1	1:1	212	272.5
5	1:1	196.2	250.2
25	1:1	186	235.2
25	1:1.2	183.4	239.2
25	1:1.4	180.3	234.1
100	1:1	187.2	245

When the milling time increased, the onset temperature decreases from 268 °C to 180 °C because most $LiNH_2$ could effectively react with LiH. The latter was explained by good contact between $LiNH_2$ and LiH particles. In the case of $LiNH_2$: LiH mole ratios increasing from 1:1 to 1:1.4, onset desorption temperature decreased because of excess LiH overcoming hydrolysis/oxidation into LiOH or Li_2O.

Furthermore, various additives and/or catalysts, such as metal hydrides (LiH, NaH, KH, MgH_2, CaH_2, and TiH_2 (Amica et al., 2015), graphite (Varin et al., 2011), nitrides, and Ti-Li-N compounds (TiN, BN and Li_5TiN_3 (Aguey-Zinsou et al., 2007), (Nayebossadri et al., 2011), (Du et al., 2015), halides ($AlCl_3$ (Ferna´ndez Albanesi et al., 2013), $MgCl_2$ (Davies et al., 2015), CeF_4

(Lin et al., 2018), KF (Dong et al., 2016), RbF (Dong et al., 2017), amide KNH_2 (Ping et al., 2019), and oxides (LiOH, NaOH, KOH (Dong et al., 2015), and $LiTi_2O_4$ (Zhang et al., 2015) have been studied to improve hydrogen sorption properties of $LiNH_2$-LiH composite. Amica et al. (2015) studied chemical interactions during hydrogen cycling of $LiNH_2$-1.6LiH doped with MH_2 (M = Mg, Ca, Ti). The results showed that $LiNH_2$ doped with MgH_2 and CaH_2 produced the solid solutions of $Li_2Mg(NH)_2$ and CaNH-$Ca(NH_2)_2$, revealing superior de/rehydrogenation kinetics (Figure 2.5). However, TiH_2 showed poorer kinetics with respect to MgH_2 - and CaH_2 – doped samples. This can be explained by the fact that TiH_2 presented direct contact with $LiNH_2$ and LiH, whereas MgH_2 and CaH_2 interacted with $LiNH_2$. Furthermore, Dong et al. (2016) reported the positive effects of potassium fluoride (KF) on the $LiNH_2$-LiH composite, in which the cycling stability of $LiNH_2$-LiH was enhanced after doping with KF (Figure 2.6).

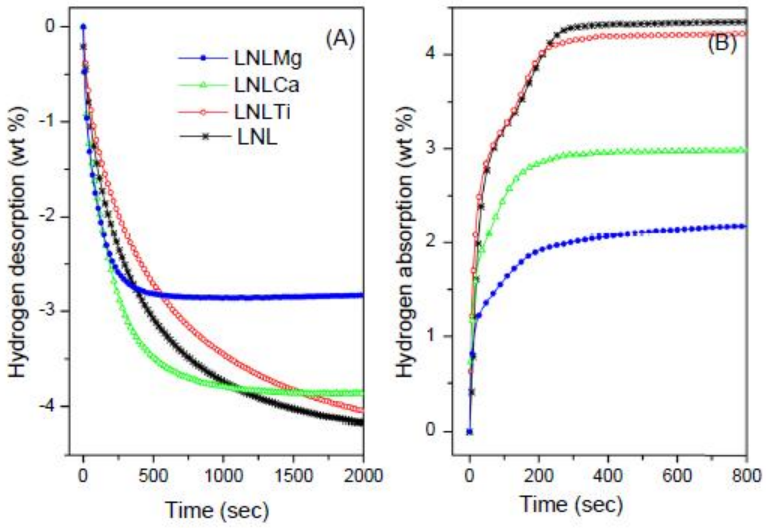

Figure 2.5 Dehydrogenation under 0.02 MPa (A) and rehydrogenation under 0.7 MPa hydrogen pressure (B) at 300 °C of the $LiNH_2$-1.6LiH and doping with MH_2 (M = Mg, Ca, and Ti).

Potassium hydride (KH) formed during ball milling of $LiNH_2$-LiH doped with KF acted as active species to improve hydrogen storage properties since it could react with NH_3 to produce KNH_2 and release hydrogen (equation 2.6).

$$KH + NH_3 \longrightarrow KNH_2 + H_2 \quad (2.6)$$

Lin et al. (2018) reported kinetic improvement of the $LiNH_2$-LiH system with 10 wt. % cerium-based materials (Ce, CeO_2, CeF_3, and CeF_4) (Figure 2.7).

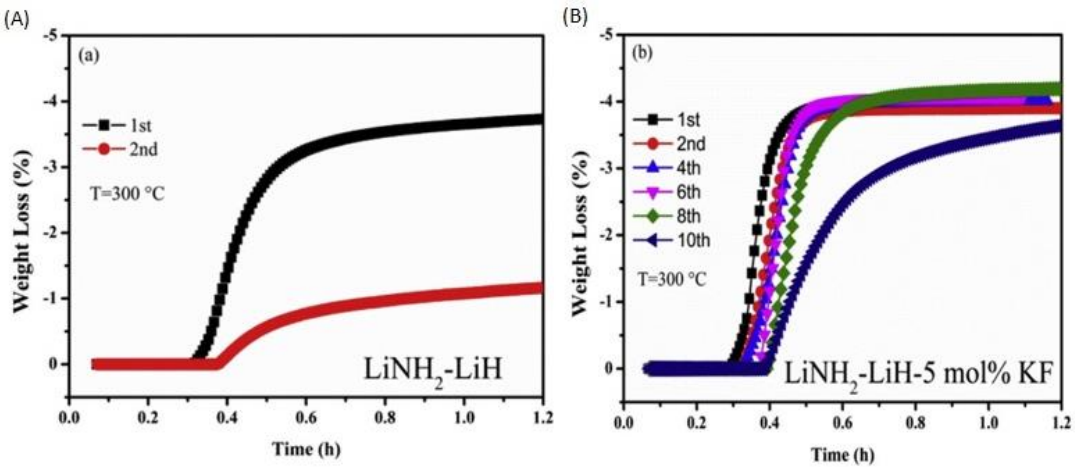

Figure 2.6 Cycling stability of $LiNH_2$-LiH (A) and $LiNH_2$-LiH-5mol%KF (B).

The best kinetic improvement and suppression of NH_3 emission was obtained from the sample doped with CeF_4. It was found that CeF_x species formed during the ball milling process was a good catalyst for $LiNH_2$ decomposition without NH_3 emission. Moreover, some active intermediate of Li_5TiN_3 found after ball milling of $LiNH_2$-LiH-Ti-based compounds (e.g., Ti, $TiCl_3$, and TiO_2) acted as NH_3 carriers from $LiNH_2$ to LiH on a nanometer scale in the forms of $Li_5TiN_3(NH_3)_x$ (Teng et al., 2011).

For carbon materials, Varin et al. (2011) proposed that doping graphite (5 wt. %) into $LiNH_2$-1.2LiH showed an increase in the de/absorbed capacities at 325 °C from 4.7 to

5.2 wt. % H_2 as well as superior reversibility with 5 wt. % H_2. It was suggested that graphite could prevent or reduce the oxidation/hydrolysis of LiH due to the water repelling from its surface. Moreover, hydrogen diffusion and heat transfer of hydride materials could be enhanced by several carbon materials, such as multi-walled carbon nanotubes (MWCNTs), activated carbon, graphene, and carbon nanofibers (CNFs).

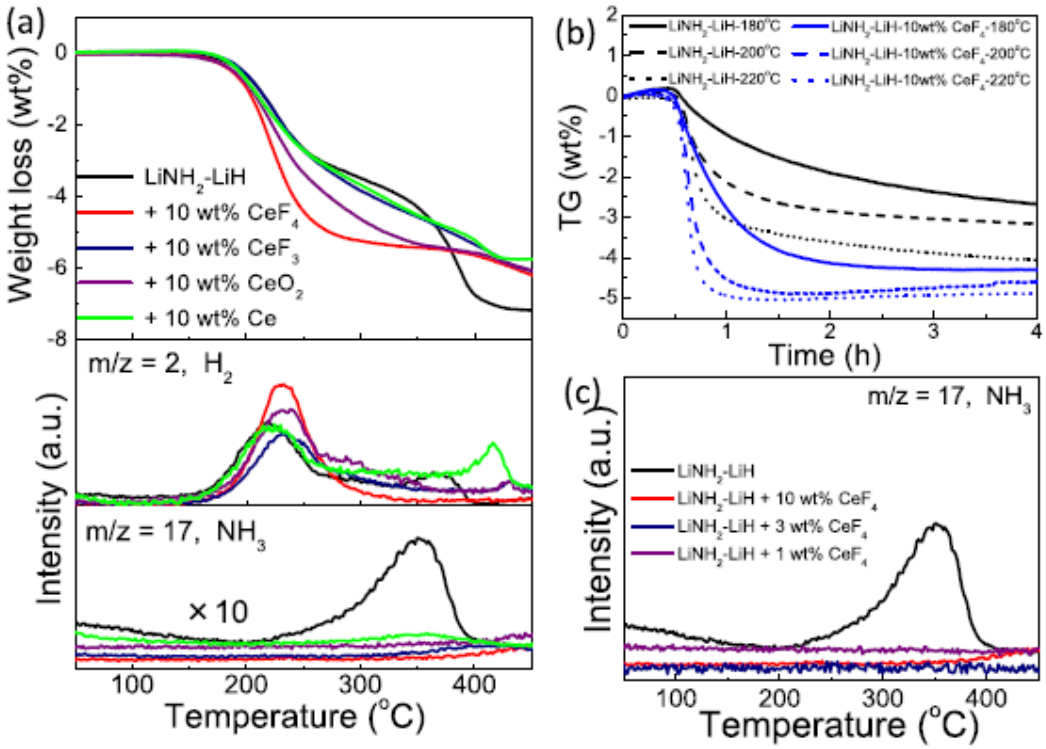

Figure 2.7 Dehydrogenation profiles of the $LiNH_2$-LiH composites and Ce- doped $LiNH_2$-LiH (a), Isothermal dehydrogenation of the $LiNH_2$-LiH composites and CeF_4-doped $LiNH_2$-LiH at different temperatures (b), and NH_3 signal in MS curves of CeF_4-doped $LiNH_2$-LiH (c).

2.3 Small hydrogen storage tanks for hydrogen storage materials

In practical applications, the hydride materials have to be packed into a closed tank. Experimental and numerical works have investigated the hydrogen sorption properties of the storage tanks. Chaise et al. (2010) and Chung et al. (2013) studied both experimental and numerical data on the de/rehydrogenation properties of the magnesium hydride-based hydrogen storage tank. They reported the enhancement of the hydrogen sorption rate by inserting heat pipes into a novel metal hydride tank. Also, heat transfer properties affecting hydrogen sorption properties were improved by inserting a heat exchanger (Wu et al., 2014). Besides tube heat exchanger, the thermal conductivity of hydride tanks was enhanced by integrating copper wire nets, aluminum foams, and hydride–graphite composites (Shim et al., 2014), (Mazzucco et al., 2014). Furthermore, the volumetric hydrogen storage capacities for hydrogen storage tanks can be enhanced by compacting metal hydride to the pellet (Lozano et al., 2011). Recently, Yan et al. (2015) designed a cylindrical lab-scale tank based on compaction of $Mg(NH_2)_2$–2LiH–0.07KOH mixed with expanded natural graphite (ENG). The laboratory-scale hydrogen storage tank was designed with 205 mm and 32 mm of length and diameter, respectively. There was a porous filter tube placed in the tank center for the hydrogen diffusion pathway. In addition, three thermocouples were located in the hydride beds for measuring the temperature during de/rehydrogenation (Figure 2.8(A)). Dehydrogenation kinetics of the compacted $Mg(NH_2)_2$–2LiH–0.07KOH mixed with up to 17 wt.% ENG were operated at 220 °C with a hydrogen flow rate of 0.6 L/min. Three regions (I, II, and III) during hydrogenation were characterized (Figure 2.8(B)). In region I, hydrogen pressure rapidly decreases and the temperature of the hydride bed is reduced when desorption occurs. For region II, the temperature decreases continuously together with hydrogen pressure drops due to the decomposition of hydrogen storage materials. The mass flow controller demonstrates hydrogen gas flows through with a constant flow rate until the pressure drops due to complete dehydrogenation.

Finally, region III is the hydrogen desorption almost finishes shown as the reduction of hydrogen flow rate less than 0.1 L/min, and the temperature in the tank increases to the set-point temperature.

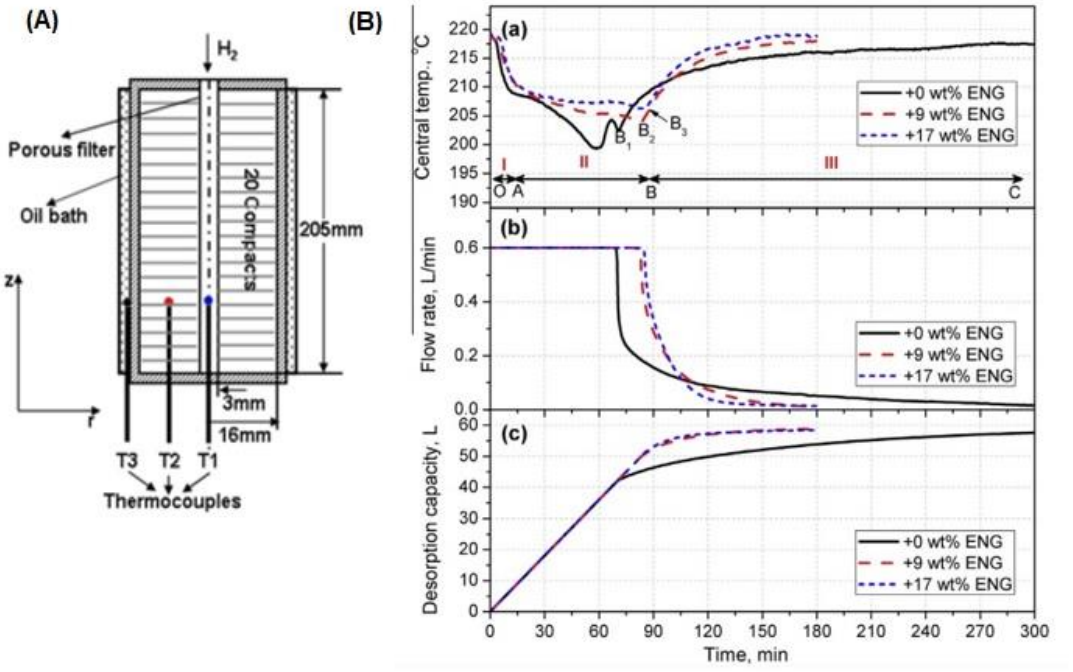

Figure 2.8 Laboratory-scale hydrogen storage tank (A) and Hydrogen desorption graph of compacted $Mg(NH_2)_2$–2LiH–0.07KOH with different ENG contents (B).

From Figure 2.8, when ENG is added in the hydride-based tank, the diffusion pathway and heat transfer of the hydride enhance. The latter results in an improvement of the hydrogen desorption process of the tank.

To the best of our knowledge, there have been no studies on the upscaling of $LiNH_2$-LiH to hydrogen storage tanks. In this study, the powder samples of $LiNH_2$-LiH will be compacted into the pellets prior to packing into the small tank to increase volumetric hydrogen capacity. However, high compaction pressure results in poor hydrogen diffusion and poor de/rehydrogenation kinetics and reversibility. Thus, catalysts and/or additives of titanium-based catalysts (TiF_4) and multi-walled carbon nanotubes (MWCNTs) will be added into $LiNH_2$-LiH. De/rehydrogenation kinetics of compacted $LiNH_2$-LiH is favored by the catalytic properties of TiF_4 as well as the improved hydrogen diffusion and thermal properties from MWCNTs (Plerdsranoy et al., 2017).

2.4 References

Aguey-Zinsou, K.F., Yao, J., Xiao G.Z. (2007). Reaction Paths between LiNH2 and LiH with Effects of Nitrides. *J. Phys. Chem. B*, *111*, 12531-12536. doi: 10.1021/jp075002l

Amica, G., Arneodo, P., and Gennari, Larochette F.C. (2015). Hydrogen storage properties of $LiNH_2$–LiH system with MgH_2, CaH_2 and TiH_2 added. *Int. J. Hydrogen Energy, 40,* 9335-9346. doi: 10.1016/j.ijhydene.2015.05.091

Chaise, A., de Rango, P., Marty, Ph., Fruchart, D. (2010). Experimental and numerical study of a magnesium hydride tank. *Int. J. Hydrogen Energy, 35,* 6311– 6322. doi: 10.1016/j.ijhydene.2010.03.057

Chen, P., Xiong, Z., Luo, J., Lin, J., and Tan, K.L. (2002). Interaction of hydrogen with metal nitrides and imides. *Nature*, *420,* 302-304. doi: 10.1038/nature01210

Chen, P., Xiong, Z., Luo, J., Lin, J., and Tan, K.L. (2003). Interaction between lithium amide and lithium hydride. *J. Phys. Chem. B, 107*, 10967-10970. doi: 10.1021/jp034149j

Chung, C.A., Yang, S.W., Yang, C.Y., Hsu C.W., and Chiu, P.Y. (2013). Experimental study on the hydrogen charge and discharge rates of metal hydride tanks using heat pipes to enhance heat transfer. *Appl. Energy, 103,* 581– 587. doi: 10.1016/j.apenergy.2012.10.024

Davies, R.A., and Anderson, P.A. (2015). Synthesis and characterization of two new amide chloride compounds: Potential H_2 storage materials. *Int. J. Hydrogen Energy, 40,* 3001-3005. doi: 10.1016/j.ijhydene.2014.12.044

Dong, B.X., Ge, J., Teng, Y.L., Gao, J.J., and Song, L. (2015). Improved dehydrogenation properties of the $LiNH_2$-LiH system by doping with alkaline metal hydroxides. *J. Mater. Chem, 3,* 905-911. doi: 10.1039/C4TA03898C

Dong, B.X., Gao, J.J., Tan, H., Teng, Y.L., Wang, L.Z., and Liu, W.L. (2016). Hydrogen desorption improvement of the $LiNH_2$-LiH-KF composite. *Int. J. Hydrogen Energy, 41,* 16122-16128. doi: 10.1016/j.ijhydene.2016.04.220

Dong, B.X., Wang, L.Z., Teng, Y.L., Li, Z.W., and Zhao, J. (2017). Superior effect of RbF on decreasing the dehydrogenation operating temperature of the $LiNH_2$-LiH system. *J. Alloys Compd, 697,* 62-67. doi: 10.1016/j.jallcom.2016.12.130

Du, L., Mauer, G., and Vaben, R. (2015). Reaction behavior of the Li-N-H hydrogen storage system with boron nitride as an additive, *Metall. Mater. Trans, 2,* 50-57. doi: 10.1007/s40553-015-0043-z

Ferna´ndez Albanesi, L, Arneodo Larochette, P., and Gennari, F.C. (2013). Destabilization of the $LiNH_2$-LiH hydrogen storage system by aluminum incorporation. *Int. J. Hydrogen Energy, 38,* 12325-12334. doi:10.1016/j.ijhydene.2013.07.030

Franklin, E.C. (1935). The nitrogen system of compounds; Reinhold, *New York*, pp53–63.

Ichikawa, T., Hanada, N., Isobe, S., Leng, H., and Fujii, H. (2004). Mechanism of Novel Reaction from $LiNH_2$ and LiH to Li_2NH and H_2 as a Promising Hydrogen Storage System. *J. Phys. Chem. B, 108,* 7887-7892. doi: 10.1021/jp049968y

Jain, A., Agarwal, S., and Ichikawa, T. (2018). Catalytic Tuning of Sorption Kinetics of Lightweight Hydrides: A Review of the Materials and Mechanism. *Catalysts, 8,* 651. doi:10.3390/catal8120651

Jebsen, J., Milanese, C., Girella, A., Lozano, G. A., Pistidda, C., Bellosta von Colbe, J. M., Marini, A., Klassen, T., and Dornheim, M. (2013). Compaction pressure influence on materials properties and sorption behavior of $LiBH_4$- MgH_2 composite. *Int. J. Hydrogen Energy,* 38, 8357-8366. doi:10.1016/j.ijhydene.2013.04.090

Juza, R., and Opp, K. (1951). Metallamide und Metallnitride 25. Mitteilung. Zur Kenntnis des Lithiumimides. *Z. Anorg. Allg. Chemie, 266*, 325–330. doi: 10.1002/zaac. 19512660607

Kojima, Y., and Kawai, Y. (2005). IR characterizations of lithiumimide and amide. *Journal of Alloys and Compounds*, *395*, 236–239. doi: 10.1016/j.jallcom.2004.10.063

Klebanoff, L. (2016). Hydrogen Storage Technology Materials and Applications, International Standard Book Number-13: 978-1-4398-4108-2 (eBook - PDF).

Lin, H. J., Li, H.W., Murakami, H., and Akiba, E. (2018). Remarkably improved hydrogen storage properties of $LiNH_2$-LiH composite via the addition of CeF_4. *Journal of Alloys and Compounds, 735,* 1017-1022. doi: 10.1016/j.jallcom.2017.10.239

Lozano, G.A., Bellosta von Colbe, J.M., Bormann, R., Klassen, T., and Dornheim, M. (2011). Enhanced volumetric hydrogen density in sodium alanate by compaction. *J. Power Sources, 196,* 9254–9259. doi: 10.1016/j.jpowsour.2011.07.053

Markmaitree, T., Ren, R., and Shaw, L.L. (2006). Enhancement of lithium amide to lithium imide transition via mechanical activation. *The Journal of Physical Chemistry B, 110,* 20710–20718. doi: 10.1021/jp060181c

Mazzucco, A., Dornheim, M., Sloth, M., Jensen, T.R., Jensen, J.O., and Rokni, M. (2014). Bed geometries, fueling strategies and optimization of heat exchanger designs in metal hydride storage systems for automotive applications: A review. *Int. J. Hydrogen Energy, 39,* 17054–17074. doi: 10.1016/j.ijhydene.2014.08.047

Modi, P., and Aguey-Zinsou, K.F. (2021). Room Temperature Metal Hydrides for Stationary and Heat Storage Applications: A Review. *Front. Energy Res,* 9, 616115. doi: 10.3389/fenrg.2021.616115

Nayebossadri, S., Aguey-Zinsou, K.F., and Guo, Z.X. (2011). Effect of nitride additives on Li-N-H hydrogen storage system. *Int. J. Hydrogen Energy, 36,* 7920-7926. doi: 10.1016/j.ijhydene.2011.01.088

Partnership, U.S.D. (2017). Target Explanation Document: Onboard Hydrogen Storage for Light-Duty Fuel Cell Vehicles. *[On-line]. Avialable:* https://www.energy.gov/sites/prod/files/2017/05/f34/fcto_targets_onboard_hydro_storage_explanation.pdf.

Ping, C., Feng, B.Q., Ge, J., Li, G.Z., Zhu, W., Teng, Y.L., Zhang, Y.R., and Dong, B.X. (2019). Cyclic reaction-induced enhancement in the dehydrogenation performances of the KNH_2-doped $LiNH_2$ and LiH system. *Int. J. Hydrogen Energy, 45,* 25927-25934. doi:https:10.1016/ j.ijhydene.2019.09.109 in press.

Plerdsranoy, P., Chanthee, S., and Utke, R. (2017). Compaction of $LiBH_4$-MgH_2 doped with MWCNTs-TiO_2 for reversible hydrogen storage. *Int. J. Hydrogen Energy, 42,* 978-986. doi: 10.1016/j.ijhydene.2016.11.066

Shaw, L.L., Osborn, W., Markmaitree, T., and Wan, X. (2008). The reaction pathway and rate limiting step of dehydrogenation of the $LiNH_2$+LiH mixture. *J. Power Sources*, *177*, 500–505. doi: 10.1016/j.jpowsour.2007.11.029

Shim, J.H., Park, M., Lee, Y.H., Kim, S., Im, Y.H., Suh, J.Y., and Cho, Y.W. (2014). Effective thermal conductivity of MgH_2 compacts containing expanded natural graphite under a hydrogen atmosphere. *Int. J. Hydrogen Energy, 39,* 349– 355. doi: 10.1016/j.ijhydene.2013.09.092

Teng, Y.L., Ichikawa, T., and Kojima, Y. (2011). Catalytic Effect of Ti-Li-N Compounds in the Li-N-H System on Hydrogen Desorption Properties. *J. Phys. Chem. C, 115*, 589-593. doi: 10.1021/jp107313r

Titherley, A.W. (1894). XLV. – Sodium, potassium, and lithium amides. *Journal of the Chemical Society, 65,* 504-522. doi: 10.1039/CT8946500504

Varin, R.A., Jang, M., and Polanskib, M. (2010). The effects of ball milling and molar ratio of LiH on the hydrogen storage properties of nanocrystalline lithium amide and lithium hydride ($LiNH_2$ + LiH) system. *Journal of Alloys and Compounds, 491,* 658–667. doi:10.1016/j.jallcom.2009.11.035

Varin, R.A., and Jang, M. (2011). The effects of graphite on the reversible hydrogen storage of nanostructured lithium amide and lithium hydride ($LiNH_2$-1.2LiH) system. *J. Alloys Compd, 509,* 7143-7151. doi: 10.1016/j.jallcom.2011.04.036

Wu, Z., Yang, F.S., Zhang, Z.X., and Bao, Z.W. (2014). Magnesium based metal hydride reactor incorporating helical coil heat exchanger: Simulation study and optimal design. *Appl. Energy, 130,* 712–722. doi: 0.1016/j.apenergy.2013.12.071

Yan, M., Sun, F., Liu, X.P., Ye, J.H., Wang, S.M., and Jiang, L.J. (2015). Effects of graphite content and compaction pressure on hydrogen desorption properties of $Mg(NH_2)_2$–2LiH based tank. *J. Alloys Compd, 628,* 63-67. doi: 10.1016/j.jallcom.2014.12.173

Zhang, T., Isobe, S., Matsuo, M., Orimo, S.I., Wang, Y., Hashimoto, N., and Ohnuki, S. (2015). Effect of Lithium Ion Conduction on Hydrogen Desorption of $LiNH_2$-LiH Solid Composite. *ACS Catal, 5,* 1552-1555. doi: 10.1021/cs501782y

Züttle, A., and Schlapbach, L. (2008). Hydrogen as a Future Energy Carrier. WILEY-VCH Verg GmbH & Co. KGaA, Weinhein, ISBN: 978-3-527-30817-0.